

Accelerating Deep Neural Network Training via Distributed Hybrid Order Optimization

Shunxian Gu^{*†}, Chaoqun You[†], Bangbang Ren^{*}, Lailong Luo^{*}, Junxu Xia^{*}, Deke Guo^{*}

^{*}National University of Defense Technology, Changsha, China

[†]Fudan University, Shanghai, China

Abstract—Scaling deep neural network (DNN) training to more devices can reduce time-to-solution. However, it is impractical for users with limited computing resources. FOSI, as a hybrid order optimizer, converges faster than conventional optimizers by taking advantage of both gradient information and curvature information when updating the DNN model. Therefore, it provides a new chance for accelerating DNN training in the resource-constrained setting. In this paper, we explore its distributed design, namely DHO₂, including distributed calculation of curvature information and model update with partial curvature information to accelerate DNN training with a low memory burden. To further reduce the training time, we design a novel strategy to parallelize the calculation of curvature information and the model update on different devices. Experimentally, our distributed design can achieve an approximate linear reduction of memory burden on each device with the increase of the device number. Meanwhile, it achieves $1.4\times \sim 2.1\times$ speedup in the total training time compared with other distributed designs based on conventional first- and second-order optimizers.

Index Terms—distributed training, hybrid order optimizer, gradient information, curvature information

I. INTRODUCTION

Deep neural network (DNN) models have given rise to numerous productive achievements in research fields such as computer vision [1], [2] and natural language processing [3], [4]. As the size of DNN models and training datasets become larger, training DNN models on a single device is increasingly time-consuming and memory-intensive. For example, finishing a 90-epoch ImageNet-1k training with ResNet-50 (20.5 million parameters) on an NVIDIA M40 GPU takes 14 days [5]. This drawback drives the development of distributed model training which scales single-device training to multiple devices. Usually, the distributed model training has three steps: (i) Replicate the entire model on each device. (ii) Each device computes a stochastic gradient on its unique mini-batch training samples in each training iteration. (iii) Each device communicates with other devices to synchronize the gradient and update its local model. This procedure repeats until the loss function converges and a certain model training accuracy is achieved. The whole training process is often referred to as the distributed synchronous stochastic gradient descent (S-SGD) algorithm. S-SGD enables a larger batch size than that of single-device training by dividing training samples into multiple devices. Therefore, it can accelerate model training when confronted with a larger dataset.

Typically, S-SGD utilizes the first-order optimizer (e.g. Adam [6], RMSProp [7]) and many prior works focus on

improving its scalability [8]–[10]. However, users with limited financial and computing resources are unable to bear the expense of renting a supercomputer for a long time to run the large-scale S-SGD. Therefore, a natural insight is to replace the optimizer by one with a higher convergence rate to accelerate model training. Recently, second-order optimizers arise since they can get a higher convergence rate than first-order ones by adding curvature information (i.e. Hessian matrix) to model update rules [11], [12]. Due to the high computational burden of calculating curvature information, most of second-order optimizers [13]–[15] select to approximate it rather than compute the accurate value. This approach sometimes amplifies the approximation error and produces noise, thus degrading the convergence speed. To solve this puzzle, FOSI (First-Order and Second-Order Integration) [16], as a hybrid order optimizer, has been proposed by minimizing the loss function with both first- and second-order optimizers. It achieves state-of-the-art model performance and convergence rate when compared with other second-order methods (e.g. K-FAC [13] and L-BFGS [17]). However, FOSI can only be employed for single-device model training at present. At this point, a natural question arises on *how to leverage the property of FOSI to accelerate the distributed model training*.

An intuitive approach is to combine FOSI with S-SGD directly by calculating curvature information on one device and broadcasting it to the others. Then, each device updates its local model with both the curvature and gradient information. However, as shown in Fig. 1a, this approach can derive two challenges: a) First, the calculation of curvature information must be finished by a single device before model update. Therefore, the other devices must keep idle until they receive the curvature information from the single device, thereby severely wasting the computational resources. b) Second, preserving the complete curvature information on each device would impose a significant memory burden. Fortunately, model parallelism [18] serves as a beneficial distributed computing technique to alleviate computational and memory burden by splitting matrix multiplication into parts across multiple devices. These two challenges and the technique motivate us to develop a distributed algorithm to accelerate model training without introducing computational resource waste and a large memory burden.

In this paper, we propose DHO₂, a FOSI-enabled distributed DNN training framework that collaboratively trains a DNN model via hybrid order optimization. In DHO₂, we first

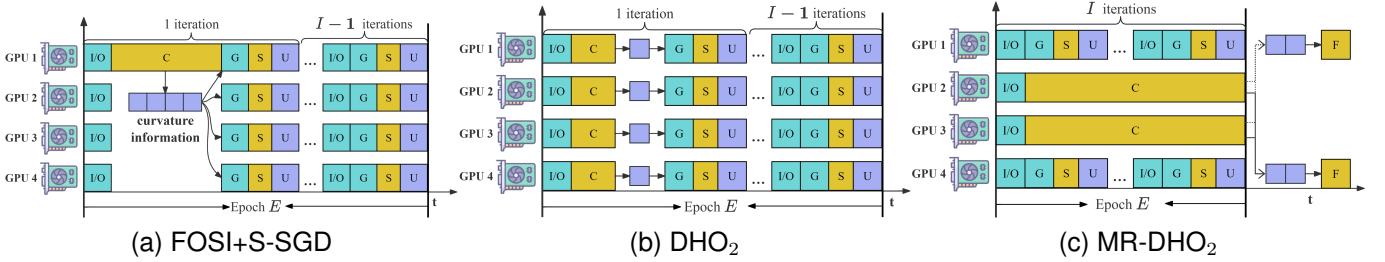


Fig. 1. The timeline of FOSI+S-SGD, DHO₂ and MR-DHO₂ in each epoch. I/O: Batch creation. C: Calculation of curvature information. G: Gradient computation. S: Gradient synchronization. U: Model update. F: Final model update at the end of each epoch. The blue box without text denotes the curvature information.

design a distributed Lanczos algorithm in curvature information calculation to reduce the computational resource waste. Specifically, by splitting the calculation of the curvature information into multiple segments and distributing them onto multiple devices, the computational resources of the devices can be effectively utilized. Next, we design a distributed model update step to enable each device to update the local model with partial curvature information rather than entire curvature information, which relieves the memory burden effectively. Most importantly, the above two designs resort to the model parallelism technique, which guarantees a computation equivalent to that in single-device training, thereby accelerating model training without degrading model performance. To further accelerate the total time per iteration, we present MR-DHO₂, a **multi-role** version of DHO₂, which classifies devices into two roles, namely accelerators and workers. A parallel algorithm is designed to enable the workers to conduct gradient computations and accelerators to calculate curvature information simultaneously. Moreover, a final model update rule is designed to combine the curvature information and gradient information for further updating the DNN model at the end of each epoch. As depicted in Fig. 1b and 1c, compared with DHO₂, MR-DHO₂ eliminates the training time for the calculation of curvature information on each worker, thereby reducing the average total training time per iteration. Our contributions can be summarized as follows:

- A FOSI-enabled distributed hybrid order optimizer framework, namely DHO₂, that allows a faster calculation of curvature information with a lower memory burden than the single-device FOSI theoretically and experimentally.
- A multi-role version of DHO₂, namely MR-DHO₂, that executes the calculation of curvature information and gradient information in parallel on different devices to further reduce the total training time per iteration.
- An evaluation of our proposed frameworks which achieve $1.4\times \sim 2.1\times$ speedup to reach a certain model performance compared with other distributed first- and second-order optimizer frameworks on a cloud server equipped with up to 32 3090 GPUs.

II. BACKGROUND

In this section, we first introduce some definitions of notations and present our problem formulation. Then, we introduce the FOSI optimization method which can only be deployed

in the single-device training and review different forms of parallelism in distributed DNN training.

A. Notations and Problem Formulation

For convenience, we unify the notations used in this paper as follows. Non-bold English and Greek letters (e.g. T, j, ϵ) denote scalars. Bold lowercase English letters (e.g. \mathbf{g}) represent vectors while bold uppercase English letters (e.g. \mathbf{H}) represent matrices. Letters in the calligraphic font (e.g. \mathcal{D}) are used to represent sets. Specially, we use $\text{diag}(\mathbf{v})$ for a diagonal matrix with arbitrary diagonal vector or entries \mathbf{v} . \odot represents the base first-order optimizer. Finally, we define a slice operator, which is a colon ":". For instance, let $\mathbf{A} \in \mathbb{R}^{N \times K \times T}$ denotes a 3-dimensional tensor, $\mathbf{A}[n_1 : n_2, k_1 : k_2, :]$ indicates a sliced sub-tensor from \mathbf{A} with N, K indexes ranging from n_1 to n_2 and k_1 to k_2 respectively. In particular, in the last dimension T , the sub-tensor takes all the entries by marking a single ":". We formulate our constrained acceleration problem as:

$$\begin{aligned} & \arg \min_{\mathbf{w}_T} Tp \\ \text{s.t. } & \frac{1}{C} \sum_{c=1}^C f(\mathbf{w}_T; \mathcal{D}_c) < \epsilon, C = G \end{aligned} \quad (1)$$

where T is the total number of training iterations and p denotes the average total training time per iteration. C is the total number of GPUs (i.e. devices) while c denotes the index of a GPU. $f(\cdot)$, \mathbf{w}_T , and \mathcal{D} denote the loss function, the final model and data samples respectively. $f(\mathbf{w}_T; \mathcal{D}_c)$ represents the loss on the data samples delivered on the c -th GPU. ϵ is the loss bound and G is the limit of the GPU number. The aim of equation 1 is to minimize the total training time of our distributed DNN training while a certain model performance is achieved and the computing resources are limited.

B. First-Order and Second-Order Integration (FOSI)

In the single-device training, gradient-based iterative optimization methods mainly encompass first-order and second-order methods. Given $\mathbf{w}_t \in \mathbb{R}^n$, the flattened model parameter vector at the t -th training iteration, both of them typically follow an update step of the form $\mathbf{w}_{t+1} = \mathbf{w}_t + \mathbf{d}_t$, where $\mathbf{d}_t \in \mathbb{R}^n$ is a descent direction determined by the current or the past first- or second-order (i.e. curvature) information. Specifically, first-order methods only use the gradient $\mathbf{g}_t = \nabla f(\mathbf{w}_t) \in \mathbb{R}^n$ while second-order methods incorporate both the gradient \mathbf{g}_t and the curvature information (i.e. the Hessian

$\mathbf{H}_t = \nabla^2 f(\mathbf{w}_t) \in \mathbb{R}^{n \times n}$, in the model update step. In the general setting of second-order methods, \mathbf{d}_t is of the form $-\eta \mathbf{P}_t^{-1} \mathbf{g}_t$, where $\mathbf{P}_t \in \mathbb{R}^{n \times n}$ is termed as a preconditioner matrix and $\eta > 0$ is a learning rate. Notably, a second-order method can be transformed into Newton’s method when $\mathbf{P}_t = \mathbf{H}_t$. However, approximating \mathbf{H}_t and then calculating its matrix inverse can result in amplifying approximation error and computational cost. To solve this puzzle, FOSI (First-Order and Second-Order Integration), a hybrid order optimizer, is proposed with three key points: a) It estimates the inverse preconditioner matrix directly, reducing approximation error and computational cost. b) It only estimates the most extreme eigenvalue and vectors of the inverse preconditioner matrix, making it more robust to noise. c) It accepts a base first-order optimizer when it maintains another Newton’s optimizer, making it suited for a variety of machine learning tasks. Then, we give an overview of FOSI, which contains four stages: the initialization stage, the warm-up stage, the extreme spectrum estimation (ESE) stage and the model update stage, and then describe the principle in each stage. Notably, our description will be emphasized on the ESE stage and model update stage since they play a key role in our distributed frameworks.

Overview. a) Like other optimization methods, FOSI starts by randomly generating the initial model parameters \mathbf{w}_0 by using a certain initialization method. b) Then, a warm-up stage is incorporated to improve the initial status of the model being trained. An appropriate initial status can prevent the curvature information calculated in the next stage from being abnormal. c) Next, in the ESE stage, the Lanczos algorithm is utilized to obtain the curvature information. d) In the model update stage, the model is iteratively updated by using the curvature information and the gradient (i.e. first-order) information simultaneously. After a pre-set number (i.e. I) of training iterations, FOSI turns back to the ESE stage to renew the curvature information and then steps into the model update stage to continue the training iterations. The ESE stage and the model update stage are repeatedly conducted until a certain model performance is achieved.

The initialization stage. Like general deep learning optimization methods, FOSI starts by initializing the model parameter vector by a certain initialization method [19], [20]. For instance, if we train a DNN model using the ReLU activation function, we should utilize the He initialization [19] to alleviate the gradient vanishment or explosion problem in the DNN training.

The warm-up stage. Since the parameters of the DNN model are randomly initialized, the value of the loss function is high at the beginning while the change of gradients is significant. As a result, the curvature (indicating the change of gradients) is extremely large, risking a numerical overflow problem. Fortunately, the curvature can be diminished with the convergence of the DNN model. Therefore, to ensure the curvature lies in a normal range, FOSI uses its base first-order optimizer to conduct a pre-set number R of model update steps

in the warm-up stage. This procedure can be represented as:

$$\mathbf{w}_R = \mathbf{w}_0 + \sum_{t=0}^{R-1} \mathbb{O}(\mathbf{g}_t) \quad (2)$$

where \mathbb{O} denotes the base first-order optimizer.

The ESE stage. Define $\hat{\mathbf{a}} \in \mathbb{R}^{k+l}$ as a vector which includes the k largest and l smallest eigenvalues of \mathbf{H}_t , and $\hat{\mathbf{V}} \in \mathbb{R}^{n \times (k+l)}$ as a matrix whose columns are the eigenvalues’ corresponding eigenvectors. Similarly, we define $\check{\mathbf{a}}$ and $\check{\mathbf{V}}$ as the vector and matrix including the rest of the eigenvalues and their corresponding eigenvectors respectively. With an identical computation result to the eigendecomposition of \mathbf{H}_t , \mathbf{H}_t can be split into two parts as follows:

$$\begin{aligned} \mathbf{H}_t &= \underbrace{\hat{\mathbf{V}} \mathbf{A}_1 \hat{\mathbf{V}}^T}_{\mathbf{H}_1} + \underbrace{\check{\mathbf{V}} \mathbf{A}_2 \check{\mathbf{V}}^T}_{\mathbf{H}_2} \\ \mathbf{A}_1 &= \text{diag}(\hat{\mathbf{a}}), \mathbf{A}_2 = \text{diag}(\check{\mathbf{a}}) \end{aligned} \quad (3)$$

The goal of the ESE stage is to obtain \mathbf{H}_1^{-1} , which is utilized in the next stage and can be represented by:

$$\mathbf{H}_1^{-1} = \hat{\mathbf{V}} \mathbf{A}_1^{-1} \hat{\mathbf{V}}^T, \mathbf{A}_1^{-1} = \frac{1}{\text{diag}(\hat{\mathbf{a}})} \quad (4)$$

The ESE stage resorts to the Lanczos algorithm [23] to achieve this goal. The key idea of the algorithm is to obtain an approximate eigendecomposition of \mathbf{H}_t . As a result, we can extract the most extreme eigenvalues and their corresponding eigenvectors from the eigendecomposition to meet the requirement of $\hat{\mathbf{a}}$ and $\hat{\mathbf{V}}$ respectively. The pseudo-code of the Lanczos algorithm is shown in algorithm 1. Specifically, the Lanczos algorithm takes the number of Lanczos iterations $m = \max\{4(k+l), 2 \ln n\}$ and an operator $hvp_t(\mathbf{v}) = \mathbf{H}_t \mathbf{v}$, $\forall \mathbf{v} \in \mathbb{R}^n$ as the input. The operator is generated by the Pearlmutter’s algorithm [24] using the loss function $f(\cdot)$ and the latest model parameter \mathbf{w}_t . In the initialization step (line 1~2 of the algorithm 1), $\mathbf{B} \in \mathbb{R}^{m \times m}$ and $\mathbf{D} \in \mathbb{R}^{n \times m}$ are initialized by creating zero matrices with the same shapes. They are ultimately a tridiagonal matrix and an orthogonal matrix (in which each column vector is a unit vector and orthogonal to each other) respectively. $\mathbf{D}[:, 1]$, which is the first column vector of \mathbf{D} , is initialized by a standard normal distribution and then normalized to a unit vector. In the arbitrary i -th Lanczos iteration, $\mathbf{B}[i, i]$ should be calculated to satisfy the following equation with \mathbf{v}_i , which is the i -th column vector of \mathbf{D} , i.e. $\mathbf{D}[:, i]$.

$$\mathbf{B}[i, i] = \mathbf{v}_i^T \underbrace{\mathbf{H}_t \mathbf{v}_i}_{hvp_t(\mathbf{v}_i)} \quad (5)$$

This equation is realized in line 4~6. Then, the Lanczos algorithm computes a vector \mathbf{h} orthogonal to \mathbf{v}_i in line 7~9, normalizes it to a unit vector in line 12 and serves it as \mathbf{v}_{i+1} . Meanwhile, in line 10~11, $\mathbf{B}[i+1, i]$ and $\mathbf{B}[i, i+1]$ are calculated to satisfy the following equations:

$$\begin{cases} \mathbf{B}[i+1, i] = \mathbf{v}_{i+1}^T \mathbf{H}_t \mathbf{v}_i = \|\mathbf{h}\|_F \\ \mathbf{B}[i, i+1] = \mathbf{v}_i^T \mathbf{H}_t \mathbf{v}_{i+1} = \|\mathbf{h}\|_F \end{cases} \quad (6)$$

Algorithm 1: Lanczos algorithm

Input : m, hvp_t ;
Output: \mathbf{D}, \mathbf{B} ;

```

1 initialization: initialize  $\mathbf{D}$  and  $\mathbf{B}$  with zero matrices;
2 initialization: randomize the column vector  $\mathbf{D}[:, 1]$  with
  standard Gaussian distribution and normalize it to a
  unit vector;
3 for  $i = 1$  to  $m$  do
4    $\mathbf{v}_i \leftarrow \mathbf{D}[:, i]$ ;
5    $\mathbf{h} \leftarrow hvp_t(\mathbf{v}_i)$ ;
6    $\mathbf{B}[i, i] \leftarrow \mathbf{h} \cdot \mathbf{v}_i$ 
7   /* Gram-Schmidt orthogonalization */
8    $\mathbf{h} \leftarrow \mathbf{h} - \mathbf{D}(\mathbf{D}^T \mathbf{h})$ 
9   /* Gram-Schmidt orthogonalization */
10   $\beta \leftarrow \|\mathbf{h}\|_F$ 
11   $\mathbf{B}[i+1, i] \leftarrow \beta$ ,  $\mathbf{B}[i, i+1] \leftarrow \beta$ 
12   $\mathbf{D}[:, i+1] \leftarrow \mathbf{h}/\beta$ 
13 end

```

After the Lanczos iterations finish, the resultant \mathbf{D} and \mathbf{B} satisfy the following equation:

$$\begin{aligned}
& \mathbf{D}^T \mathbf{H}_t \mathbf{D} = \mathbf{B} \\
& \Leftrightarrow \underbrace{\mathbf{D} \mathbf{D}^T}_{\mathbf{I}} \mathbf{H}_t \underbrace{\mathbf{D} \mathbf{D}^T}_{\mathbf{I}} = \mathbf{D} \mathbf{B} \mathbf{D}^T \quad (7) \\
& \Leftrightarrow \mathbf{H}_t = \mathbf{D} \mathbf{B} \mathbf{D}^T
\end{aligned}$$

since \mathbf{D} is an orthogonal matrix whose columns are formed by $\{\mathbf{v}_i\}_{i=1}^m$. By taking the eigendecomposition of \mathbf{B} , we can get the following equation:

$$\mathbf{H}_t = \mathbf{D} \mathbf{U} \mathit{diag}(\mathbf{u}) \mathbf{U}^T \mathbf{D}^T \Leftrightarrow \mathbf{H}_t = \underbrace{(\mathbf{D} \mathbf{U})}_{\mathbf{Z}} \mathit{diag}(\mathbf{u}) \underbrace{(\mathbf{D} \mathbf{U})^T}_{\mathbf{Z}} \quad (8)$$

where \mathbf{u} is the vector formed by the eigenvalues of \mathbf{B} and \mathbf{U} is the matrix whose columns are the corresponding eigenvectors of the eigenvalues. Since not all the eigenvalues in \mathbf{u} are the approximation of the eigenvalues in \mathbf{H}_t , the equation 8 is an approximate eigendecomposition of \mathbf{H}_t . However, the most extreme values in \mathbf{u} can converge to the real most extreme eigenvalues of \mathbf{H}_t with the increase of m . Finally, we can get the required $\hat{\mathbf{a}}$ and $\hat{\mathbf{V}}$ in the equation 4 by extracting the k largest and l smallest entries from \mathbf{u} and selecting their corresponding eigenvectors from \mathbf{Z} . \mathbf{H}_1^{-1} is thus obtained.

The model update stage. FOSI iteratively updates the model using \mathbf{H}_1^{-1} obtained in the last stage and the gradient information in the current training iteration. Specifically, in the arbitrary t -th training iteration, FOSI computes the stochastic gradient \mathbf{g}_t and implicitly uses the second-order Taylor's expansion of f , i.e. $\tilde{f} = f_t + (\mathbf{w} - \mathbf{w}_t)^T \mathbf{g}_t + \frac{1}{2}(\mathbf{w} - \mathbf{w}_t)^T \mathbf{H}_t (\mathbf{w} - \mathbf{w}_t)$, where f_t is the loss in the t -th training iteration. Then, it splits \tilde{f} into two parts as follows:

$$f_1 = \frac{1}{2} f_t + (\mathbf{w} - \mathbf{w}_t)^T \mathbf{g}_1 + \frac{1}{2} (\mathbf{w} - \mathbf{w}_t)^T \mathbf{H}_1 (\mathbf{w} - \mathbf{w}_t) \quad (9)$$

$$f_2 = \frac{1}{2} f_t + (\mathbf{w} - \mathbf{w}_t)^T \mathbf{g}_2 + \frac{1}{2} (\mathbf{w} - \mathbf{w}_t)^T \mathbf{H}_2 (\mathbf{w} - \mathbf{w}_t) \quad (10)$$

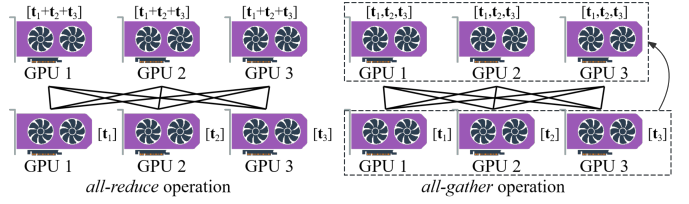


Fig. 2. Synchronization techniques in distributed DNN training when the overall number of GPUs is 3.

where \mathbf{g}_1 is the sum of \mathbf{g}_t 's projections on $\hat{\mathbf{V}}$'s columns, i.e. $\mathbf{g}_1 = \hat{\mathbf{V}}(\hat{\mathbf{V}}^T \mathbf{g}_t)$ while \mathbf{g}_2 is the sum of \mathbf{g}_t 's projections on $\hat{\mathbf{V}}$'s columns, i.e. $\mathbf{g}_2 = (\mathbf{I} - \hat{\mathbf{V}}\hat{\mathbf{V}}^T)\mathbf{g}_t = \mathbf{g}_t - \mathbf{g}_1$. Since \mathbf{g}_2 can be regarded as the Gram-Schmidt orthogonalization of \mathbf{g}_t on $\hat{\mathbf{V}}$'s column vectors, \mathbf{g}_2 is orthogonal to each column vector of $\hat{\mathbf{V}}$. We can infer that \mathbf{g}_2 is orthogonal to \mathbf{g}_1 because \mathbf{g}_1 is the linear combination of the column vectors in $\hat{\mathbf{V}}$. Next, FOSI optimizes f by minimizing f_1 and f_2 independently. For f_1 , FOSI uses a α -scaled Newton's step. The Newton's step is obtained by putting the derivatives of the equation 9 on \mathbf{w} to 0, and is α -scaled as follows:

$$\begin{aligned}
\mathbf{w}^* &= \mathbf{w}_t - \mathbf{H}_1^{-1} \mathbf{g}_1 \\
\Delta_1 &= -\alpha \mathbf{H}_1^{-1} \mathbf{g}_1 \quad (11) \\
&= -\alpha (\hat{\mathbf{V}}(\mathbf{A}_1^{-1}(\hat{\mathbf{V}}^T \mathbf{g}_1)))
\end{aligned}$$

where Δ_1 denotes the descent vector calculated by Newton's step and it is a linear combination of $\hat{\mathbf{V}}$'s column vectors and thus is orthogonal to \mathbf{g}_2 . Meanwhile, FOSI uses the base first-order optimizer to minimize f_2 . Since certain first-order optimizers (e.g. Adam [6]) can change the direction of \mathbf{g}_2 , to maintain the orthogonality of $\mathcal{O}(\mathbf{g}_2)$ to Δ_1 , $\mathcal{O}(\mathbf{g}_2)$ is further transformed by Gram-Schmidt orthogonalization as follows:

$$\begin{aligned}
\Delta_2 &= (\mathbf{I} - \hat{\mathbf{V}}\hat{\mathbf{V}}^T) \mathcal{O}(\mathbf{g}_2) \\
&= \mathcal{O}(\mathbf{g}_2) - \hat{\mathbf{V}}(\hat{\mathbf{V}}^T \mathcal{O}(\mathbf{g}_2)) \quad (12) \\
&= \mathcal{O}(\mathbf{g}_t - \mathbf{g}_1) - \hat{\mathbf{V}}(\hat{\mathbf{V}}^T \mathcal{O}(\mathbf{g}_t - \mathbf{g}_1))
\end{aligned}$$

where Δ_2 denotes the descent vector calculated by the base first-order optimizer. Finally, in the arbitrary t -th training iteration, the model update step is mathematically represented as $\mathbf{w}_{t+1} = \mathbf{w}_t + \Delta_1 + \Delta_2$.

C. Data Parallelism and Model Parallelism

Data parallelism and model parallelism are the typical methods utilized in distributed DNN training across multiple devices. Data parallelism, which S-SGD uses, enables remaining the same model on each device. In each training iteration, a unique mini-batch is consumed by each device to compute a stochastic gradient. Then, all devices synchronize their gradients by an *all-reduce* operation, in which each device broadcasts its gradient to all the other devices and sums its received gradients as depicted in Fig. 2, followed by an average operation. Finally, a unified gradient can be obtained and devices use it to update their local models at the end of each iteration. Data parallelism is the most common choice for scaling single-device training to multiple devices. Model

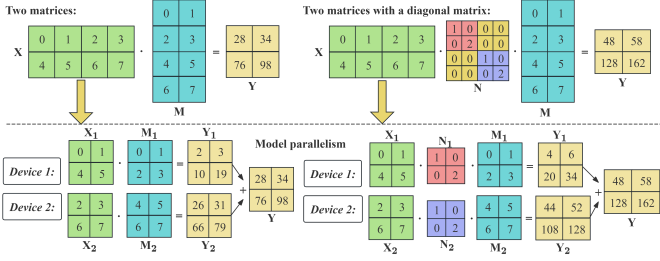


Fig. 3. Model parallelism. The crucial concept lies in slicing the matrix onto multiple devices for concurrent matrix multiplications, thereby alleviating the computational burden of matrix multiplications executed by a single device.

parallelism is primarily targeted at circumstances where matrices are overly large, preventing matrix operations (i.e. matrix multiplication) from being conducted on a single device. As depicted in Fig. 3, the main notion of model parallelism is to slice the multiplier and multiplicand onto multiple devices to realize the parallel matrix product while ensuring the same output result as the original matrix multiplication. Furthermore, as illustrated in Fig. 3, the application scenarios of model parallelism are categorized into two kinds, specialized for the matrix multiplication of two matrices and for that of two matrices with a diagonal matrix respectively. In the rest of this paper, if not specially stated, the model parallelization technique is generally referred to as the former kind.

III. DESIGN OF DHO₂

In this section, we start by designing the distributed Lanczos algorithm for the ESE stage and the distributed model update step for the model update stage. Then, we present the operating flow of DHO₂ and give a theoretical analysis on the computation complexity, and memory burden.

A. Distributed Lanczos Algorithm

As the model becomes deeper and wider, the number of model parameters n becomes extremely large. As a result, it is unaffordable for the memory space of a single GPU to store $\mathbf{D} \in \mathbb{R}^{n \times m}$. Therefore, the target of the distributed Lanczos algorithm is to remain partial \mathbf{D} on each GPU and each GPU can achieve an incomplete $\hat{\mathbf{V}}$ at the end of the ESE stage. The pseudo-code of the distributed Lanczos algorithm is shown in algorithm 2, where s_c and e_c are the split start point and the split end point on the c -th GPU. In general, $e_c - s_c + 1 = n/C$. Specifically, different from the original Lanczos algorithm, each GPU only initializes its part of \mathbf{D} in line 1 and fixes the first column vector partially in line 3. Then, in the arbitrary i -th Lanczos iteration, each GPU gathers the partial i -th column vectors from the other GPUs to form the complete \mathbf{v}_i so that $\mathbf{B}[i, i]$ can be updated by using the equation 5 (in line 5~line 7). The model parallelism technique is introduced in the following Gram-Schmidt orthogonalization (line 8~ line 11) to obtain a correct but partial \mathbf{h} , with $\mathbf{h}[s_c : e_c]$ and $\mathbf{D}[s_c : e_c, :]$. At the end of the Lanczos iteration, since each GPU stores a partial \mathbf{h} , the Frobenius norm of \mathbf{h} should be obtained by calculating the l_2 norm of $\mathbf{h}[s_c : e_c]$ on each GPU and synchronizing it with an *all-reduce* operation. The square root of the synchronization result is the required

Algorithm 2: distributed Lanczos algorithm

Input : m, hvp_t ;

Output: $\mathbf{D}[s_c : e_c, :], \mathbf{B}$;

- 1 initialization: initialize $\mathbf{D}[s_c : e_c, :]$ and \mathbf{B} with zero matrices; randomize \mathbf{v}_1 by standard Gaussian distribution with a same random seed and normalize it to a unit vector;
- 2 **for** $c = 1$ **to** C **in parallel do**
- 3 $\mathbf{D}[s_c : e_c, 1] = \mathbf{v}_1[s_c : e_c]$
- 4 **for** $i = 1$ **to** m **do**
- 5 $\mathbf{v}_i \leftarrow \text{all_gather}(\{\mathbf{D}[s_c : e_c, i]\}_{c=1}^C)$;
- 6 $\mathbf{h} \leftarrow hvp_t(\mathbf{v}_i)$;
- 7 $\mathbf{B}[i, i] \leftarrow \mathbf{h} \cdot \mathbf{v}_i$
- 8 /* Gram-Schmidt orthogonalization */
- 9 $\mathbf{m} \leftarrow \text{all_reduce}(\{\mathbf{D}[s_c : e_c, :]^T \mathbf{h}[s_c : e_c]\}_{c=1}^C)$
- 10 $\mathbf{h}[s_c : e_c] \leftarrow \mathbf{h}[s_c : e_c] - \mathbf{D}[s_c : e_c, :]\mathbf{m}$
- 11 /* Gram-Schmidt orthogonalization */
- 12 $\beta \leftarrow \sqrt{\text{all_reduce}(\{\|\mathbf{h}[s_c : e_c]\|_2^2\}_{c=1}^C)}$
- 13 $\mathbf{B}[i + 1, i] \leftarrow \beta$, $\mathbf{B}[i, i + 1] \leftarrow \beta$
- 14 $\mathbf{D}[s_c : e_c, i + 1] \leftarrow \mathbf{h}[s_c : e_c] / \beta$
- 15 **end**
- 16 **end**

Frobenius norm, as in line 12~13. The $(i + 1)$ -th partial column vector of \mathbf{D} on each GPU is updated by the normalized $\mathbf{h}[s_c : e_c]$, as in line 14. After finishing the Lanczos iterations, the distributed Lanczos algorithm obtains the same \mathbf{B} as the original Lanczos algorithm and the partial \mathbf{D} , i.e. $\mathbf{D}[s_c : e_c, :]$. Next, we decompose the \mathbf{B} to $\mathbf{U} \text{diag}(\mathbf{u}) \mathbf{U}^T$ as in the original Lanczos algorithm. Finally, we can get the required $\hat{\mathbf{a}}$ and a partial $\hat{\mathbf{V}}$, i.e. $\hat{\mathbf{V}}[s_c : e_c, :] \in \mathbb{R}^{n/C \times (k+l)}$ by extracting the k largest and l smallest entries from \mathbf{u} and selecting its corresponding partial column vectors from $\mathbf{D}[s_c : e_c, :]\mathbf{U}$. Thanks to the model parallelism technique, the computation process in the distributed Lanczos algorithm is identical to that in the original one.

B. Distributed Model Update Step

After DHO₂ completes the ESE stage, it steps into the model update stage, whose aim is to update the local model with partial curvature information on each GPU iteratively. Most importantly, it should achieve the identical computation process to the equation 11 and the equation 12. However, the partial $\hat{\mathbf{V}}$ obtained in the previous distributed Lanczos algorithm cannot be directly utilized to compute the \mathbf{g}_1 in the equation 11 by the model parallelism technique. That is because the second dimensionality of the partial $\hat{\mathbf{V}}$'s transpose cannot fit the first one of \mathbf{g}_t , obstructing the calculation $\mathbf{g}_1 = \hat{\mathbf{V}}(\hat{\mathbf{V}}^T \mathbf{g}_t)$, where $\hat{\mathbf{V}}$ is replaced with $\hat{\mathbf{V}}[s_c : e_c, :]$. As a result, DHO₂ must conduct the following reconstruction before starting the training iterations. Specifically, we evenly partition the partial $\hat{\mathbf{V}}$ to C parts in the second dimensionality on each GPU. As illustrated in Fig. 4, one of the parts is the remaining part for the c -th GPU while the other parts, i.e.

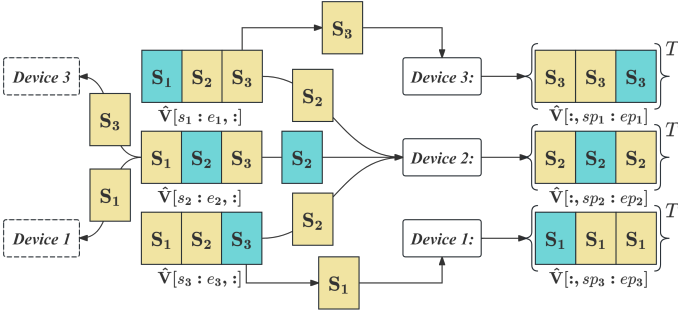


Fig. 4. The transformation of the partial $\hat{\mathbf{V}}$ to our required one when the overall number of GPUs is 3. The cyan square is the remaining part while the beige square is the scattered part.

$\{\mathbf{S}_c\}_{c=1}^C - \{\mathbf{S}_c\}$, $\mathbf{S}_c \in \mathbb{R}^{(n/C) \times ((k+l)/C)}$, are scattered to the other GPUs. After each GPU receives the parts from the other GPUs, it can generate a new partial $\hat{\mathbf{V}}$, i.e. $\hat{\mathbf{V}}[:, 1 + (c-1)(k+l)/C : 1 + c(k+l)/C]$ which can support the following model update step conducted in each training iteration. For convenience, we conduct the redefinition: $1 + (c-1)(k+l)/C \stackrel{\text{def}}{=} sp_c$ and $1 + c(k+l)/C \stackrel{\text{def}}{=} ep_c$, where sp_c and ep_c are all scalars. We present the distributed model update step of each training iteration in algorithm 3 which takes $\hat{\mathbf{a}}$, $\hat{\mathbf{V}}[:, sp_c : ep_c]$ and \mathbf{w}_t as input. Specifically, at the beginning of each iteration (line 2), each GPU computes a stochastic gradient \mathbf{g}_t on its batch of data samples and synchronizes it with an *all-reduce* operation with averaging. Then (line 3 ~ 4), DHO₂ computes the sum of \mathbf{g}_t 's projection on $\hat{\mathbf{V}}$'s columns, i.e. \mathbf{g}_1 on each device and the matrix multiplications involved are conducted by the model parallelism technique. Next (line 5 ~ 7), Δ_1 can be obtained with the same computation process as the equation 11 by using the model parallelism technique specialized for the matrix multiplication of two matrices with a diagonal matrix. Finally, Δ_2 is achieved with the identical computation process to the equation 12 via the same model parallelism technique used for calculating \mathbf{g}_1 (in line 8 ~ 10) and the local model is updated by using Δ_1 and Δ_2 at the end of each training iteration (in line 11). The training iteration is repeatedly executed until a pre-set number (i.e. I) of that is reached.

C. Operating Flow of DHO₂

Based on the proposed distributed Lanczos algorithm and the distributed model update step, we describe the operating flow of DHO₂, which can be regarded as a distributed implementation of FOSI. Specifically, **a) the initialization stage**: DHO₂ initializes the DNN model like general deep learning optimization methods and replicates it on each GPU. Then, it steps into **b) the warm-up stage**, in which it conducts the model update step as in S-SGD by using its base first-order optimizer until a pre-set number of training iterations is reached. The warm-up stage can prevent the curvature information obtained in the next stage from being abnormal. Next, it resorts to the distributed Lanczos algorithm **c) in the ESE stage** to obtain partial curvature information (i.e. $\hat{\mathbf{a}}$ and $\hat{\mathbf{V}}[s_c : e_c, :]$) on each GPU. Finally, in **d) the model update stage**, each GPU reconstructs its partial curvature information (from $\hat{\mathbf{V}}[s_c : e_c, :]$ to $\hat{\mathbf{V}}[:, sp_c : ep_c]$) and then

Algorithm 3: distributed model update step

Input : $\hat{\mathbf{a}}$, $\hat{\mathbf{V}}[:, sp_c : ep_c]$, \mathbf{w}_t ;

Output: \mathbf{w}_{t+1} ;

```

1 for  $c = 1$  to  $C$  in parallel do do
2    $\mathbf{g}_t = \text{all\_reduce}(\{\nabla f(\mathbf{w}_t; \mathcal{D}_c)\}_{c=1}^C) / C$ 
3    $\mathbf{g}_1 = (\hat{\mathbf{V}}[:, sp_c : ep_c] (\hat{\mathbf{V}}[:, sp_c : ep_c]^T \mathbf{g}_t))$ 
4    $\mathbf{g}_1 = \text{all\_reduce}(\{\mathbf{g}_1\}_{c=1}^C)$ 
5    $\mathbf{A}_1^{-1} = \frac{1}{\text{diag}(\hat{\mathbf{a}}[sp_c : ep_c])}$ 
6    $\mathbf{n} = -\alpha (\hat{\mathbf{V}}[:, sp_c : ep_c] (\mathbf{A}_1^{-1} (\hat{\mathbf{V}}[:, sp_c : ep_c]^T \mathbf{g}_1)))$ 
7    $\Delta_1 = \text{all\_reduce}(\mathbf{n})$ 
8    $\mathbf{g}_2 = \mathbf{g}_t - \mathbf{g}_1$ 
9    $\mathbf{s} = (\hat{\mathbf{V}}[:, sp_c : ep_c] (\hat{\mathbf{V}}[:, sp_c : ep_c]^T \mathbb{O}(\mathbf{g}_2)))$ 
10   $\Delta_2 = \mathbb{O}(\mathbf{g}_2) - \text{all\_reduce}(\{\mathbf{s}\}_{c=1}^C)$ 
11   $\mathbf{w}_{t+1} = \mathbf{w}_t + \Delta_1 + \Delta_2$ 
12 end

```

steps into training iterations. In each training iteration, each GPU conducts the distributed model update step to update the local model with gradient information and partial curvature information. When the number of training iterations reaches a pre-set number, DHO₂ turns back to the ESE stage to update the curvature information and then enters the model update stage again. This procedure of the ESE stage and the model update stage is repeatedly executed until the model converges.

D. Computation and Memory

Before we start the complexity analysis of DHO₂ with the original FOSI, we first denote the number of epochs as E and assume that each epoch contains I training iterations. In other words, DHO₂ and the original FOSI start the ESE stage at the beginning of each epoch. Meanwhile, since both DHO₂ and the original FOSI compute stochastic gradients in their model update step, it is unnecessary to take the computational complexity of the gradient computation into consideration.

Computational complexity analysis: The disparity between DHO₂ and the original FOSI resides in the incorporation of model parallelism in the Gram-Schmidt orthogonalization and model update step. In the Gram-Schmidt orthogonalization of the original FOSI, the computation in line 8 of algorithm 1 requires a complexity of $\mathcal{O}(2mn + n)$. Meanwhile, in line 9 ~ 10 of algorithm 2, by remaining partial \mathbf{D} on each GPU, the computational complexity of each GPU becomes $\mathcal{O}((2m + 1)(n/C))$. On the other hand, the model update step in the original FOSI requires a complexity of $\mathcal{O}(4(k+l)n + (k+l)^2)$ and $\mathcal{O}(2n(k+l+1))$ in the equation 11 and 12. Meanwhile, its distributed implementation (i.e. algorithm 3) has a complexity of $\mathcal{O}(\frac{(k+l)}{C}(6n + \frac{k+l}{C}) + 2n)$ in total on each GPU. Therefore, the total reduction of the computational complexity from FOSI to DHO₂ on each GPU is $\mathcal{O}((2m+1)(n - n/C) + I((\frac{(k+l)(C-1)}{C})6n + \frac{(k+l)^2(C^2-1)}{C^2}))$ in each epoch.

Memory burden analysis. As mentioned in the section III-A, the key idea of alleviating the memory burden in FOSI is to reduce the memory usage of \mathbf{D} , which occupies the largest

memory usage compared with other objects. In the original FOSI, the complexity of the memory burden caused by \mathbf{D} is $\mathcal{O}(mn)$ while the complexity is reduced to $\mathcal{O}(mn/C)$ on each GPU thanks to splitting \mathbf{D} onto C GPUs.

IV. DESIGN OF MR-DHO₂

In this section, we first present an overview of the proposed MR-DHO₂ and give a detailed description of its components. Finally, we give a theoretical analysis on why MR-DHO₂ has a shorter total training time per iteration than DHO₂.

A. Overview of MR-DHO₂

The bottleneck of DHO₂ is that it should further post-process the computed gradient in the distributed model update step of each training iteration, thereby introducing extra time consumption. Meanwhile, the ESE stage at the beginning of each epoch can increase the average total training time per iteration. To this end, we heuristically propose MR-DHO₂, a multi-role version of DHO₂, which classifies devices (i.e. GPUs) into two roles, accelerators and workers, respectively. Our proposed DHO₂ and previous works like SSO [21] and KAISA [22] must finish the calculation of curvature information before updating the model on each device. Different from them, the key idea of MR-DHO₂ is to parallelize the calculation of curvature information for accelerators with the model update steps using a first-order optimizer for workers in each epoch. Specifically, MR-DHO₂ follows the same initialization stage and warm-up stage as DHO₂. Then, in each epoch, the workers conduct model update steps by merely using a first-order optimizer while the accelerators conduct the calculation of curvature information. At the end of each epoch, the workers utilize the curvature information to generate the latest model through a final model update. The epoch repeats until the model converges.

B. Accelerators and Workers

Accelerators: At the beginning of each epoch, the accelerators receive the latest model parameter (i.e. \mathbf{w}_{EI}) from any one of the workers and start the ESE stage by using the distributed Lanczos algorithm proposed in the section III-A. After completing the ESE stage, each accelerator can get $\hat{\mathbf{a}}$ and a partial $\hat{\mathbf{V}}$ i.e. $\hat{\mathbf{V}}[s_a : e_a, :]$ where a is the index of an accelerator. Each accelerator further evenly partitions the obtained $\hat{\mathbf{V}}[s_a : e_a, :]$ into J parts (i.e. $\{\hat{\mathbf{V}}[s_a : e_a, sp_j : ep_j] \stackrel{def}{=} \mathbf{R}_j\}_{j=1}^J$) in the second dimensionality, where j is the index of a worker and J is the total number of workers. Then, as illustrated in Fig. 5, each accelerator scatters the partitioned parts onto the workers and finally each worker arranges its received parts in order and concatenates them in the first dimensionality to obtain $\hat{\mathbf{V}}[:, sp_j : ep_j]$. Meanwhile, $\hat{\mathbf{a}}$ is broadcasted by any one of the accelerators to all workers. Both $\hat{\mathbf{a}}$ and $\hat{\mathbf{V}}[:, sp_j : ep_j]$ are the required curvature information of the final model update on the workers at the end of each epoch.

Workers: At the beginning of each epoch, each worker sets the latest model parameter vector \mathbf{w}_t as the checkpoint i.e. $\mathbf{c} = \mathbf{w}_t$ and initializes a zero vector $\mathbf{p} \in \mathbb{R}^n$. Then, in each training iteration, each worker computes a stochastic

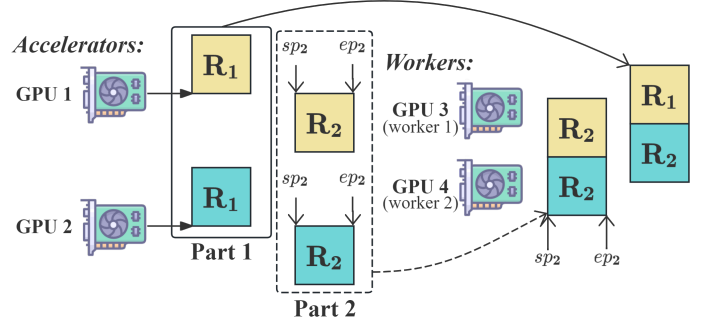


Fig. 5. An example of the accelerators scattering the resultant curvature information to the workers. The beige squares are the partitioned parts of GPU 1 while the cyan squares are that of GPU 2.

gradient i.e. $\mathbf{g}_t = \nabla f(\mathbf{w}_t)$ and synchronizes it by an all-reduce operation with averaging. It utilizes it to update its model by using its base first-order optimizer. Meanwhile, the synchronized gradient is added to \mathbf{p} , which is used in the final model update. This training process in each training iteration can be mathematically represented as follows.

$$\begin{aligned} \mathbf{w}_{t+1} &= \mathbf{w}_t + \mathbb{O}(\text{all_reduce}(\mathbf{g}_t)) \\ \mathbf{p}_{t+1} &= \begin{cases} \mathbf{p}_t + \text{all_reduce}(\mathbf{g}_t), & \text{if } t \bmod I \neq 0 \\ 0, & \text{if } t \bmod I = 0 \end{cases} \end{aligned} \quad (13)$$

After completing the training iterations, each worker receives and reconstructs the curvature information from the accelerators. With the checkpoint \mathbf{c} , the accumulated vector \mathbf{p} and the partial curvature information (i.e. $\hat{\mathbf{a}}$ and $\hat{\mathbf{V}}[:, sp_j : ep_j]$), the workers can conduct the final model update at the end of each epoch as described in the following subsection.

C. Final Model Update

We heuristically present the final model update rule at the end of each epoch to combine the curvature information from the accelerators and the gradient information from the workers for further updating the model. Specifically, with a synchronized gradient \mathbf{g}_t in the arbitrary t -th training iteration, we can formulate the training process in each epoch as follows:

$$\mathbf{w}_{(E+1)I} = \underbrace{\mathbf{w}_{EI}}_{\mathbf{c}} + \sum_{t=EI+1}^{(E+1)I} (\Delta_1 + \Delta_2) \quad (14)$$

where the sum of Δ_1 can be further split into:

$$\begin{aligned} \sum_{t=EI+1}^{(E+1)I} \Delta_1 &= -\alpha \sum_{t=EI+1}^{(E+1)I} \mathbf{H}_1^{-1} \mathbf{g}_t \\ &= -\alpha \sum_{t=EI+1}^{(E+1)I} \sum_{j=1}^J \underbrace{\hat{\mathbf{V}}[:, sp_j : ep_j]}_{\mathbf{v}} \mathbf{A}_1^{-1} \hat{\mathbf{V}}[:, sp_j : ep_j]^T \mathbf{g}_t \\ &= -\alpha \sum_{t=EI+1}^{(E+1)I} \sum_{j=1}^J \mathbf{v} \mathbf{A}_1^{-1} \underbrace{\mathbf{v}^T \mathbf{v}}_{\mathbf{I}} \mathbf{v}^T \mathbf{g}_t \\ &= -\alpha \sum_{j=1}^J \mathbf{v} \mathbf{A}_1^{-1} \mathbf{v}^T \underbrace{\sum_{t=EI+1}^{(E+1)I} \mathbf{g}_t}_{\mathbf{p}} \end{aligned} \quad (15)$$

where $\mathbf{g}_1 = \sum_{j=1}^J \mathbf{V}\mathbf{V}^T \mathbf{g}_t$, $\mathbf{A}_1^{-1} = \frac{1}{\text{diag}(\hat{\mathbf{a}}_{[sp_j:ep_j]})}$ and \mathbf{p} can be the biased estimation of the sum of \mathbf{g}_t . That is because the \mathbf{g}_t here is modified by the curvature information in each training iteration while \mathbf{p} uses the original gradient information calculated by a first-order optimizer. Then, the sum of Δ_2 can be split into:

$$\begin{aligned} \sum_{t=EI+1}^{(E+1)I} \Delta_2 &= \sum_{t=EI+1}^{(E+1)I} (\mathbf{I} - \sum_{j=1}^J \mathbf{V}\mathbf{V}^T) \odot (\mathbf{g}_2) \\ &= (\mathbf{I} - \sum_{j=1}^J \mathbf{V}\mathbf{V}^T) \sum_{t=EI+1}^{(E+1)I} \odot (\mathbf{g}_t - \mathbf{g}_1) \\ &\approx (\mathbf{I} - \sum_{j=1}^J \mathbf{V}\mathbf{V}^T) (\mathbf{I} - \sum_{j=1}^J \mathbf{V}\mathbf{V}^T) \underbrace{\left(\sum_{t=EI+1}^{(E+1)I} \odot (\mathbf{g}_t) \right)}_{\mathbf{w}'_{EI+I} - \mathbf{c}} \end{aligned} \quad (16)$$

where \mathbf{w}'_{EI+I} is the updated model parameter in the last training iteration of each epoch. Based on the last equations in the equation 15 and 16, the final model update on each worker can be mathematically represented as:

$$\begin{aligned} \mathbf{w}_{(E+1)I} &= \mathbf{c} - \alpha \sum_{j=1}^J (\mathbf{V}(\mathbf{A}_1^{-1}(\mathbf{V}^T \mathbf{p}))) \\ &+ (\mathbf{I} - \sum_{j=1}^J \mathbf{V}\mathbf{V}^T) (\mathbf{I} - \sum_{j=1}^J \mathbf{V}\mathbf{V}^T) \underbrace{(\mathbf{w}'_{EI+I} - \mathbf{c})}_{\mathbf{o}} \\ &= \mathbf{c} - \alpha \sum_{j=1}^J (\mathbf{V}(\mathbf{A}_1^{-1}(\mathbf{V}^T \mathbf{p}))) \\ &+ \mathbf{o} - \sum_{j=1}^J \mathbf{V}(\mathbf{V}^T \mathbf{o}) - \sum_{j=1}^J \mathbf{V}(\mathbf{V}^T (\mathbf{o} - \sum_{j=1}^J \mathbf{V}(\mathbf{V}^T \mathbf{o}))) \end{aligned} \quad (17)$$

where each sum operation $\sum_{j=1}^J$ represents an all-reduce operation within the workers.

D. Theoretical Analysis

As described in the section III-D, the total computational complexity of DHO₂ in one epoch caused by the distributed model update steps is $\mathcal{O}(I(\frac{(k+l)}{C}(6n + \frac{k+l}{C}) + 2n))$. Meanwhile, MR-DHO₂ does not require the distributed model update step to post-process \mathbf{g}_t in each training iteration. Only the final model update introduces extra computational complexity in each epoch and the complexity is $\mathcal{O}(\frac{(k+l)}{C}(8n + \frac{k+l}{C}) + 6n)$, which is about 3 distributed model update steps in DHO₂. Therefore, as long as $I > 3$ (which is easy to satisfy in the practical setting), MR-DHO₂ requires a greatly shorter total training time per epoch than DHO₂. In other words, the average total training time per iteration can be significantly reduced from DHO₂ to MR-DHO₂.

V. EXPERIMENTS

A. Experimental Settings

Testbed. We implement our proposed distributed DNN training frameworks on a cloud server which is equipped with

32 NVIDIA®GeForce®RTX 3090 GPUs. Each GPU is linked by PCIe with a bandwidth of 936.2 GB/s.

Models and dataset. To evaluate our frameworks' generalization, we implement them on a variety of DNN models with different structures, including DenseNet-201, VGG-16, Swin-Transformer-t, Swin-Transformer-s, ResNet-34 and ResNet-101 [2], [25], [26]. The parameter number of these DNN models ranges from 18.1 million (DenseNet-201) to 49.6 million (Swin-Transformer-s). All DNN models are learned from scratch except for the Swin-Transformer which is pre-trained on the ImageNet dataset [27] and we conduct fine-tuning on it. Meanwhile, we consider the image classification task on the CIFAR-10 dataset [28], which contains 60,000 tiny images. Each image has a resolution of 32×32 and can be classified into 10 categories.

Baselines and metrics. To evaluate the speedup of our frameworks using a hybrid order optimizer, we compare them with the original FOSI and other distributed first- and second-order optimizer frameworks. The total training time to achieve an accuracy of 90% [29] on the CIFAR-10 dataset is utilized as the main metric while the total training time per iteration and memory cost are also taken into account. Specifically, in our first experiment, we compare DHO₂ with the original FOSI to evaluate the effectiveness of our distributed design on accelerating training time and alleviating memory burden, which is discussed in the section III-D. In our second experiment, we compare DHO₂ and MR-DHO₂ with distributed first-order (Adam [6] and RMSProp [7]) and second-order (K-FAC [11]) optimizer frameworks to prove the superiority of our frameworks on the training time. By the way, regardless of whether our experiment is conducted in a single-device or multi-device setting, the total batch size is consistently set to 256 since this value can achieve the best convergence speed empirically. In MR-DHO₂, 50% of the GPUs are treated as the accelerators since this ratio can eliminate the bubble in the parallelization at large.

B. Comparison with Original FOSI

In order to prove that DHO₂ has a lower computational complexity and memory burden than the original FOSI, we implement them on training DenseNet-201. Fig. 6 demonstrates the test accuracy versus training epoch curve, the total training time per epoch and the peak memory usage of DHO₂ and the original FOSI. The curve shows that DHO₂ requires 8 ~ 10 training epochs to achieve 90% accuracy while the original FOSI needs 12 epochs. The total training epochs of them are close. That is because the introduction of the model parallelism technique enables DHO₂ to have the same computation process as the original FOSI. As a result, DHO₂ has the same convergence rate as the original FOSI. Meanwhile, DHO₂ has a shorter total training time per epoch than the original FOSI, verifying our computational complexity analysis in the section III-D. However, with the increase of the GPU number, the total training time per epoch does not exhibit a linear downward trend. This is because the introduction of more GPUs can result in an extra communication burden. Finally, the peak

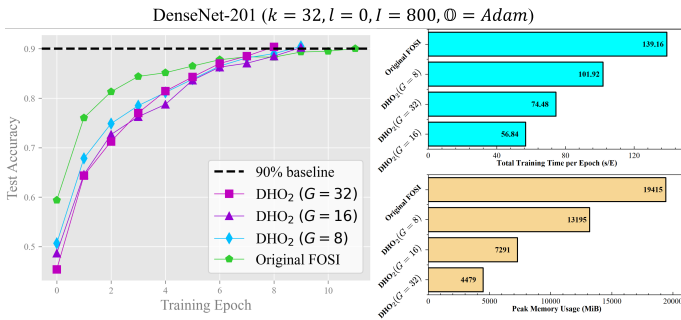


Fig. 6. The model performance, total training time per epoch and peak memory usage of DHO₂ and the original FOSI.

memory usage exhibits an approximate linear reduction since each GPU can store a smaller piece of the matrix \mathbf{D} with the increase of GPU number, as discussed in the section III-D.

C. Comparison with First- and Second-Order Optimizers

To evaluate our hybrid order frameworks’ speedup relative to first-order optimizer frameworks, we first compare DHO₂ and MR-DHO₂ with S-SGD using the Adam optimizer and S-SGD using RMSProp optimizer. Fig. 8 demonstrates the test accuracy versus training epoch curve while Fig. 9 shows the total training time and the training iteration time (i.e. the total training time per iteration) of each framework. In Fig. 8, we can find that DHO₂ requires the least training epochs on training comparatively small models (i.e. ResNet-34 and Swin-Transformer-t) while MR-DHO₂ requires the least ones on training comparatively large models (i.e. ResNet-101 and Swin-Transformer-s). That is because DHO₂ utilizes accurate curvature information to post-process gradient information in each training iteration. Thus, the gradient information in each training iteration is an accurate one too. However, MR-DHO₂ heuristically uses biased estimations on the sum of gradients and the descent direction of \mathbf{g}_2 in the equation 14 and 15 respectively. Consequently, although DHO₂ converges faster than MR-DHO₂ in principle thanks to the introduction of less error, it is more prone to over-fitting problems when confronted with complex DNN structures. Furthermore, DHO₂ and MR-DHO₂ consume the shortest total training time on training comparatively small model and large model respectively, as shown in Fig. 9. They achieve about $1.4\times \sim 1.8\times$ speedup compared with the first-order optimizer frameworks. However, DHO₂ has a longer training iteration time than all frameworks. This is because it conducts the distributed model update step in each training iteration to post-process the gradient information while the other frameworks only need the gradient information. Meanwhile, MR-DHO₂ can reduce 6% \sim 17% training iteration time of DHO₂ since it parallelizes the calculation of curvature and gradient information. It reduces the training iteration time to the level of the first-order optimizer frameworks, verifying our theoretical analysis in the section IV-D. Last but not least, thanks to the superiority of FOSI in the convergence rate, although DHO₂ and MR-DHO₂ require a longer training iteration time, this drawback can be compensated by fewer training epochs.

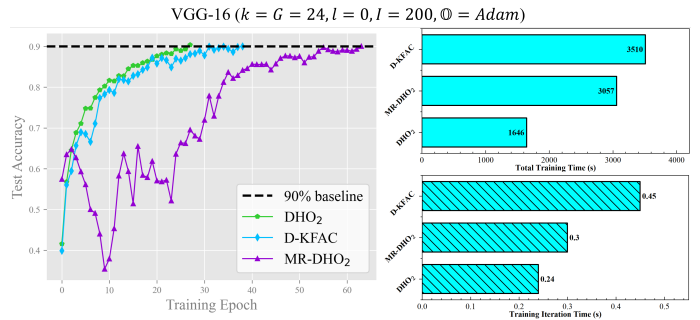


Fig. 7. The model performance, total training time and training iteration time of DHO₂, MR-DHO₂ and D-KFAC when we train VGG-16.

We also compare DHO₂ and MR-DHO₂ with the well-known second-order optimizer framework, namely distributed K-FAC (D-KFAC). Fig. 7 shows the test accuracy versus training epoch curve, the total training time and the training iteration time of each framework on training VGG-16. It shows that both DHO₂ and MR-DHO₂ outperform D-KFAC in the total training time. That is because their prototype (i.e. FOSI) originally converges faster than the prototype of D-KFAC (i.e. K-FAC). Meanwhile, DHO₂ has the same convergence rate as the original FOSI, as discussed in the section V-B, resulting in a shorter total training time than D-KFAC. On the other hand, MR-DHO₂ can influence the convergence rate of the original FOSI but it has a shorter training iteration time than DHO₂. This advantage compensates for the loss of convergence rate and thus MR-DHO₂ also requires a shorter total training time than D-KFAC. Finally, MR-DHO₂ converges slower than DHO₂ when training VGG-16. This is because the size of VGG-16 (33.6 million parameters) is close to that of ResNet-34 (21.9 million parameters). As mentioned in the last subsection, DHO₂ converges faster than MR-DHO₂ when confronted with a comparatively small DNN structure.

VI. CONCLUSIONS

In this paper, we have explored the distributed design of a hybrid order optimizer, namely FOSI. Specifically, we have proposed a distributed DNN training framework using a hybrid order optimizer, namely DHO₂. It incorporates the distributed Lanczos algorithm to accelerate the calculation of curvature information and the distributed model update step to reduce memory burden. To further reduce the training iteration time, we have further proposed MR-DHO₂, which parallelizes the calculation of curvature information and the model update step. Experimentally, our distributed design can significantly reduce the memory burden on each device compared with the original FOSI in the single-device setting. Meanwhile, it achieves $1.4\times \sim 2.1\times$ speedup in the total training time compared with other conventional first-order and second-order optimizer frameworks.

REFERENCES

- [1] M. Dehghani, J. Djolonga, B. Mustafa, P. Padlewski, J. Heek, J. Gilmer, A. P. Steiner, M. Caron, R. Geirhos, I. Alabdulmohsin *et al.*, “Scaling vision transformers to 22 billion parameters,” in *International Conference on Machine Learning*. PMLR, 2023, pp. 7480–7512.

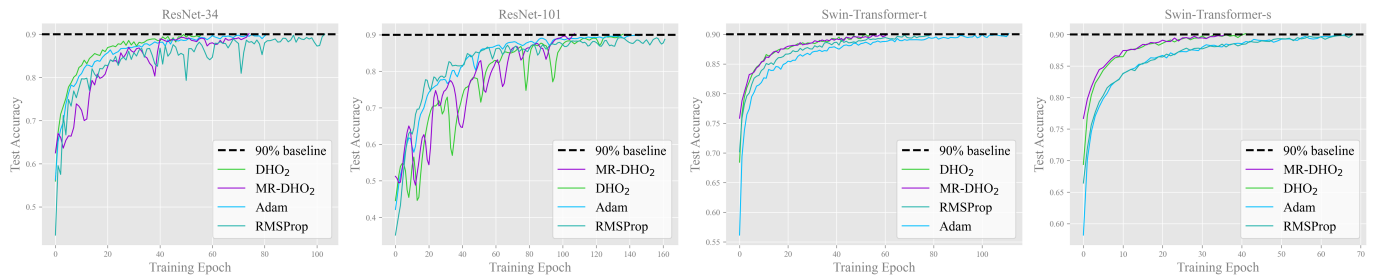


Fig. 8. The test accuracy versus training epoch curve when we train ResNet and Swin-Transformer ($K = G = 24, l = 0, I = 200, \textcircled{O} = Adam$).

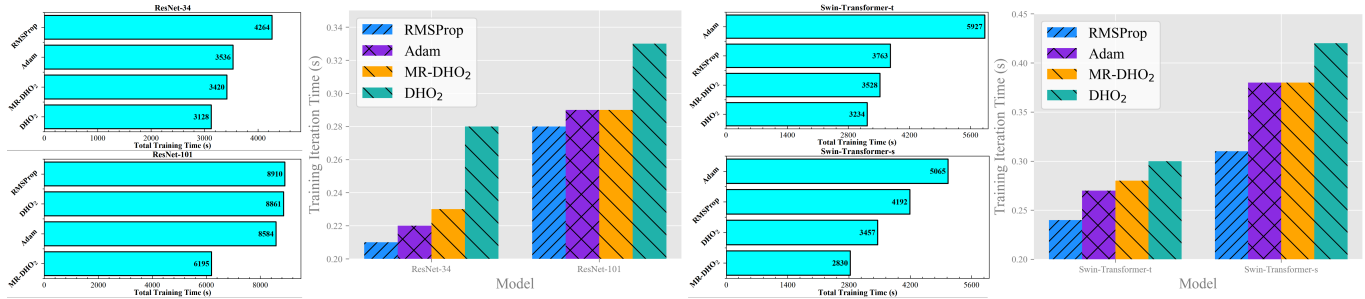


Fig. 9. The total training time and the training iteration time of our frameworks and other first-order optimizer frameworks.

[2] K. He, X. Zhang, S. Ren, and J. Sun, "Deep residual learning for image recognition," in *Proceedings of the IEEE conference on computer vision and pattern recognition*, 2016, pp. 770–778.

[3] J. D. M.-W. C. Kenton and L. K. Toutanova, "Bert: Pre-training of deep bidirectional transformers for language understanding," in *Proceedings of naacL-HLT*, vol. 1. Minneapolis, Minnesota, 2019, p. 2.

[4] T. Brown, B. Mann, N. Ryder, M. Subbiah, J. D. Kaplan, P. Dhariwal, A. Neelakantan, P. Shyam, G. Sastry, A. Askell *et al.*, "Language models are few-shot learners," *Advances in neural information processing systems*, vol. 33, pp. 1877–1901, 2020.

[5] Y. You, Z. Zhang, C.-J. Hsieh, J. Demmel, and K. Keutzer, "Imagenet training in minutes," in *Proceedings of the 47th international conference on parallel processing*, 2018, pp. 1–10.

[6] D. P. Kingma, "Adam: A method for stochastic optimization," *arXiv preprint arXiv:1412.6980*, 2014.

[7] G. Hinton, N. Srivastava, and K. Swersky, "Neural networks for machine learning lecture 6a overview of mini-batch gradient descent," *Cited on*, vol. 14, no. 8, p. 2, 2012.

[8] P. Goyal, "Accurate, large minibatch sg d: training imagenet in 1 hour," *arXiv preprint arXiv:1706.02677*, 2017.

[9] L. Bottou, F. E. Curtis, and J. Nocedal, "Optimization methods for large-scale machine learning," *SIAM review*, vol. 60, no. 2, pp. 223–311, 2018.

[10] Y. You, J. Hseu, C. Ying, J. Demmel, K. Keutzer, and C.-J. Hsieh, "Large-batch training for lstm and beyond," in *Proceedings of the International Conference for High Performance Computing, Networking, Storage and Analysis*, 2019, pp. 1–16.

[11] J. G. Pauloski, L. Huang, W. Xu, K. Chard, I. T. Foster, and Z. Zhang, "Deep neural network training with distributed k-fac," *IEEE Transactions on Parallel and Distributed Systems*, vol. 33, no. 12, pp. 3616–3627, 2022.

[12] H.-J. M. Shi, T.-H. Lee, S. Iwasaki, J. Gallego-Posada, Z. Li, K. Rangadurai, D. Mudigere, and M. Rabbat, "A distributed data-parallel pytorch implementation of the distributed shampoo optimizer for training neural networks at-scale," *arXiv preprint arXiv:2309.06497*, 2023.

[13] J. Martens and R. Grosse, "Optimizing neural networks with kronecker-factored approximate curvature," in *International conference on machine learning*. PMLR, 2015, pp. 2408–2417.

[14] V. Gupta, T. Koren, and Y. Singer, "Shampoo: Preconditioned stochastic tensor optimization," in *International Conference on Machine Learning*. PMLR, 2018, pp. 1842–1850.

[15] H. Sivan, M. Gabel, and A. Schuster, "Automon: Automatic distributed monitoring for arbitrary multivariate functions," in *Proceedings of the 2022 International Conference on Management of Data*, 2022, pp. 310–324.

[16] S. Hadar, G. Moshe, and S. Assaf, "Fosi: Hybrid first and second order optimization," in *The Twelfth International Conference on Learning Representations*, 2024.

[17] D. C. Liu and J. Nocedal, "On the limited memory bfgs method for large scale optimization," *Mathematical programming*, vol. 45, no. 1, pp. 503–528, 1989.

[18] M. Shoenybi, M. Patwary, R. Puri, P. LeGresley, J. Casper, and B. Catanzaro, "Megatron-lm: Training multi-billion parameter language models using model parallelism," *arXiv preprint arXiv:1909.08053*, 2019.

[19] K. He, X. Zhang, S. Ren, and J. Sun, "Delving deep into rectifiers: Surpassing human-level performance on imagenet classification," in *Proceedings of the IEEE international conference on computer vision*, 2015, pp. 1026–1034.

[20] X. Glorot and Y. Bengio, "Understanding the difficulty of training deep feedforward neural networks," in *Proceedings of the thirteenth international conference on artificial intelligence and statistics. JMLR Workshop and Conference Proceedings*, 2010, pp. 249–256.

[21] R. Anil, V. Gupta, T. Koren, K. Regan, and Y. Singer, "Scalable second order optimization for deep learning," *arXiv preprint arXiv:2002.09018*, 2020.

[22] J. G. Pauloski, Q. Huang, L. Huang, S. Venkataraman, K. Chard, I. Foster, and Z. Zhang, "Kaisa: An adaptive second-order optimizer framework for deep neural networks," in *Proceedings of the International Conference for High Performance Computing, Networking, Storage and Analysis*, 2021, pp. 1–14.

[23] C. Lanczos, "An iteration method for the solution of the eigenvalue problem of linear differential and integral operators," 1950.

[24] B. A. Pearlmutter, "Fast exact multiplication by the hessian," *Neural computation*, vol. 6, no. 1, pp. 147–160, 1994.

[25] K. Simonyan and A. Zisserman, "Very deep convolutional networks for large-scale image recognition," *arXiv preprint arXiv:1409.1556*, 2014.

[26] Z. Liu, Y. Lin, Y. Cao, H. Hu, Y. Wei, Z. Zhang, S. Lin, and B. Guo, "Swin transformer: Hierarchical vision transformer using shifted windows," in *Proceedings of the IEEE/CVF international conference on computer vision*, 2021, pp. 10012–10022.

[27] J. Deng, W. Dong, R. Socher, L.-J. Li, K. Li, and L. Fei-Fei, "Imagenet: A large-scale hierarchical image database," in *2009 IEEE conference on computer vision and pattern recognition*. Ieee, 2009, pp. 248–255.

[28] A. Krizhevsky, G. Hinton *et al.*, "Learning multiple layers of features from tiny images," 2009.

[29] I. Garg, S. S. Chowdhury, and K. Roy, "Dct-snn: Using dct to distribute spatial information over time for low-latency spiking neural networks," in *Proceedings of the IEEE/CVF International Conference on Computer Vision*, 2021, pp. 4671–4680.